Measurement of Visible Emission from Laser-Produced Sn Plasma in Hydrogen Atmosphere

Shusen GAO[1)]*, Keishin WATANABE[1)], Yu TAKEHIRO[1)], Yuito NISHII[1)], Maki KISHIMOTO[1)], Tomoyuki JOHZAKI[1,2)], Atushi SUNAHARA[2,3)], Kotaro YAMASAKI[1)], Takeshi HIGASHIGUCHI[4)], Shinichi NAMBA[1)]

[1)] *Graduate School of Advanced Science and Engineering, Hiroshima University, 1-3-2 Kagamiyama, Higashihiroshima, Hiroshima 739-8527, Japan*
[2)] *Institute of Laser Engineering, Osaka University, 2-6 Yamadaoka, Suita, Osaka 565-0871, Japan*
[3)] *Center for Material under Extreme Environment, Purdue University, 610 Purdue Mall, West Lafayette, IN 47907, U.S*
[4)] *Department of Electrical and Electronic Engineering, Utsunomiya University, 350 Minemachi Utsunomiya, Tochigi 321-8505, Japan*

(Received 30 August 2025 / Accepted 20 November 2025)

Laser-produced tin (Sn) plasma is extensively used as an extreme ultraviolet (EUV) light source for advanced lithography; however, the collector mirror lifetime is considerably shortened by high-energy debris from the plasma. The introduction of hydrogen (H_2) gas into the plasma region can mitigate debris through ion–neutral collisions and chemical reactions forming gaseous stannane (SnH_4). However, the detailed Sn-H interaction mechanisms remain uninvestigated. Herein, visible emission spectroscopy was used to investigate the spatiotemporal behaviors of Sn and H plasmas generated by 12-ps, 1,064-nm laser pulses incident on a solid Sn target in a 100 Pa H_2 atmosphere. Spatiotemporal-resolved measurements of H_α and H_β lines revealed prompt hydrogen excitation following plasma generation, with electron temperatures of 1–2 eV and electron densities up to 1×10^{17} cm^{-3} near the target. These conditions aid the formation of hydrogen radicals that react with Sn atoms/ions to produce SnH_4, contributing to the effective mitigation of debris. These findings offer insights into the optimization of the EUV source performance and the prolongation of the optical component lifetime.

Keywords: laser-produced plasma, tin plasma, hydrogen gas, EUV lithography, debris removal, plasma spectroscopy, electron temperature, electron density

DOI: 10.1585/pfr.21.2406016

1. Introduction

Extreme ultraviolet (EUV) lithography at 13.5 nm is a crucial technology for fabricating semiconductor devices with sub-20-nm features. Among the various EUV sources, laser-produced tin (Sn) plasma offers high conversion efficiency and is used in mass production. However, it generates debris, including fast neutral atoms and highly charged ions. These particles cause severe damage and contamination of Mo/Si multilayer collector mirrors, thereby reducing their lifetime from the required 12 months to only a few months.

Several mitigation strategies have been proposed and studied. Among them, the introduction of hydrogen (H_2) gas into plasma chambers is promising [1–3]. Collisions between hydrogen atoms/molecules and energetic Sn ions can reduce the ion charge states and kinetic energies. Moreover, electrons are cooled owing to elastic and inelastic collisions with the ambient gas. Meanwhile, chemical reactions between neutral Sn and hydrogen radicals form volatile stannane (SnH_4), which can be pumped out of vacuum chambers. Despite its simplicity and effectiveness, the detailed interaction processes between Sn and H/H_2 remain uninvestigated [4–6].

This study aims to investigate the spatiotemporal behaviors of Sn atoms/ions and atomic hydrogen in Sn–H_2 laser plasmas by analyzing visible emission spectroscopy. Further, the electron density and expansion velocity are evaluated using H Balmer lines.

2. Experimental Setup

Experiments were conducted using a Nd:YAG laser system (λ: 1,064 nm, pulse width: 12 ps, pulse energy: < 35 mJ). The laser beam was directed into a vacuum chamber and focused onto a solid Sn plate target of a 1-mm thickness. A plano-convex fused silica lens with a focal length of f = 100 mm was employed. The focal spot size was estimated to be 50 μm (full width at half maximum: FWHM), corresponding

*Corresponding author's e-mail: m244478@hiroshima-u.ac.jp
This article is based on the presentation at the Joint Conference of the 22nd International Conference on Atomic Processes in Plasmas (APiP 2025) and 1st NIFS Conference on Atomic and Molecular Processes in Plasmas.

to a laser intensity of 10^{12}–10^{13} W/cm^2, sufficient to generate Sn plasma.

The vacuum chamber was evacuated using a dry pump (Kashiyama NeoDry36E) and a turbomolecular pump (Osaka Vacuum TG350FVAB) to a base pressure of approximately 1×10^{-3} Pa. Subsequently, H_2 (purity: 99.999%) was introduced via a mass flow controller (KOFLOC 3660A) to achieve a pressure of 100 ± 2 Pa, which was monitored using an absolute vacuum pressure gauge (Mykrolis MODEL P-10).

The target, focusing lens, and a 0.2-mm-thick glass debris shield were mounted on a four-axis motorized stage inside the vacuum chamber, allowing precise movement of the target along the *x*-, *y*-, and *z*-axes and rotation around its vertical axis. The *x*-, *y*-, and *z*-axes correspond to the laser propagation, horizontal, and vertical directions, respectively (Fig. 1).

For spatially resolved spectroscopic diagnostics, a linear array of 48 quartz fiber bundles (core diameter: 250 μm, length: 3 m) was arranged along the target normal direction to capture plasma plume expansion (Fig. 2). The fiber array covered a spatial range of approximately 30 mm from the target surface. The target surface was imaged onto the fiber end faces using an achromatic lens (f = 150 mm) with a demagnification factor of approximately 3.4:1, while the other bundle fiber end was coupled to the spectrometer entrance slit via an achromatic lens (f = 200 mm, 1:1 magnification). Each fiber channel's spatial resolution was determined to be approximately 0.6 mm.

For plasma diagnostics, the electron temperature (Te) was determined based on Boltzmann plots of the population densities of several Sn I and Sn II excited states. To this end, a relative intensity calibration of the entire optical system was performed using an Xe standard lamp, by which the spectral intensity (CCD count) was converted to the relative population density. Table 1 shows the Sn I and II spectra used for the Boltzmann plots, as well as H_α and H_β. The electron density was obtained from the Stark broadening width of the H_β line (486 nm). A low-pressure H_2 lamp was used to estimate the instrumental width. Monitoring the hydrogen Balmer lines, H_α (656 nm) and H_β (486 nm), enabled us to investigate the atomic process and dynamic behavior of hydrogen induced by Sn plasma.

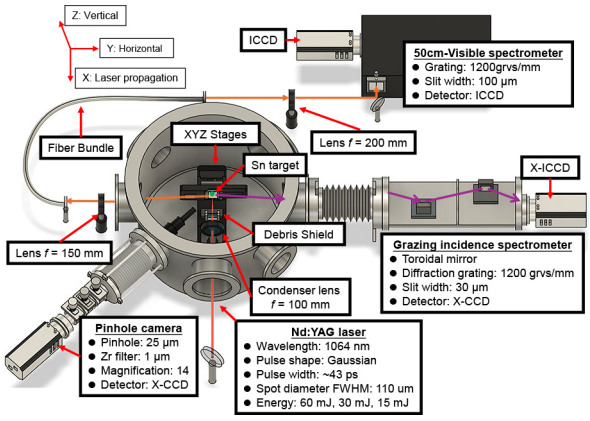

Fig. 1. Schematic of the experimental setup for visible and EUV emission spectroscopies.

Table 1. Spectral lines of Sn I and II excited states and hydrogen Balmer lines for Boltzmann plot.

Species	Wavelength (nm)	Transition
Sn I	452.47	5p ^{1}S → 6s ^{1}P^0
Sn II	457.90	4f ^{2}F^0 → 6g ^{2}G
Sn III	485.84	6s ^{3}S → 6p ^{3}P^0
Sn II	533.23	6p ^{2}P^0 → 6d ^{2}D
Sn II	556.19	6p ^{2}P^0 → 6d ^{2}D
Sn II	558.88	5d ^{2}D → 4f ^{2}F^0
Sn II	579.88	5d ^{2}D → 4f ^{2}F^0
H	486.13	2 → 4
H	656.27	2 → 3

3. Results and Discussion

Time-integrated plasma emissions were recorded in vacuum and H_2 gas environments (Fig. 3). The plasma predominantly emitted green light in the vacuum atmosphere owing to strong Sn I and II transitions. The plasma was approximately 40 mm extended from the target. Meanwhile, the hydrogen atmosphere generated a range of emission colors, starting with white and blue near the target, transitioning to pink further out owing to hydrogen excitation. These color changes are linked to atomic hydrogen generation and electronic excitation, resulting in the Balmer series emissions (H_β and H_γ lines).

Figure 4 shows the Te profiles as a function of the distance from the target in vacuum (Fig. 4(a)) and H_2 atmospheres (Fig. 4(b)). In vacuum, Te was approximately 4 eV at 90 ns,

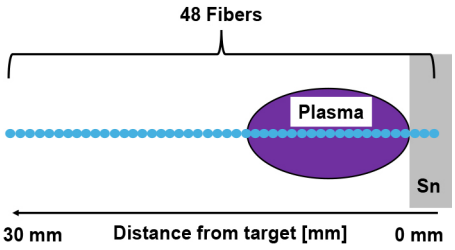

Fig. 2. Positional relationship between 48-core bundle fiber and laser-produced Sn plasma image.

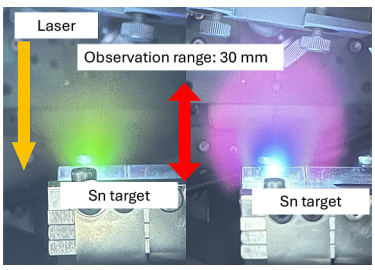

Fig. 3. Photograph of Sn laser plasmas [left: in vacuum; right: in hydrogen atmosphere (100 Pa)].

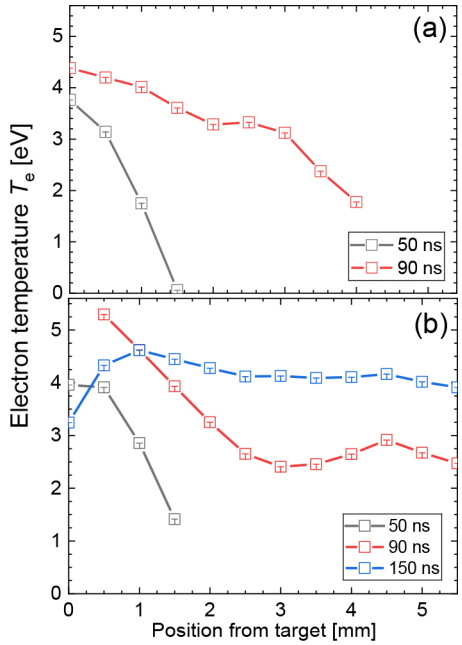

Fig. 4. Distance dependence of electron temperature after laser irradiation in (a) vacuum and (b) H_2 gas.

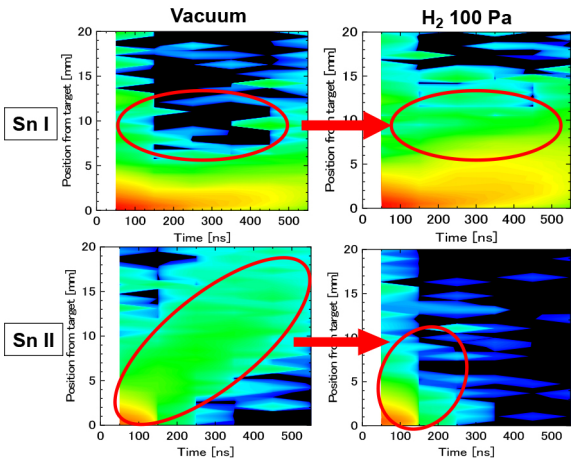

Fig. 5. Spatiotemporal distribution of emission intensity at different laser intensities.

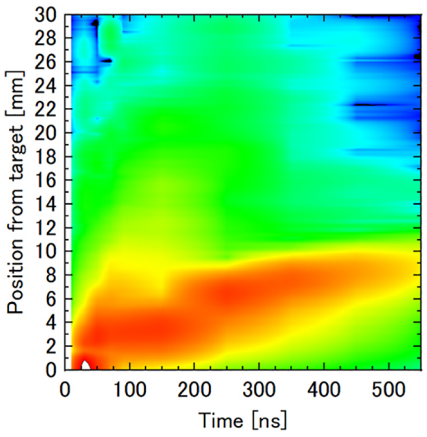

Fig. 6. Spatiotemporal distribution of H_α emission intensity.

consistent with previous studies [7], whereas the Sn emission became too weak for evaluation at later times. In hydrogen, Te at 50 ns was similar to that in vacuum; however, the temperature for 90 ns was higher by ~ 1 eV than that in vacuum. During and immediately after laser irradiation in vacuum, two particle energy components exists: thermal- and low-temperature plasma and shifted Maxwellian plasma with narrow- and high-energy distribution [8]. In H_2, the latter hot energy electrons are cooled owing to collision with the ambient gas and are rapidly thermalized. Consequently, the temperature increases (Fig. 4(b)). Notably, the temperature estimated using the Boltzmann plot method corresponds to low-energy thermal plasma. Meanwhile, for a 90-ns time delay, it decreases linearly but increases again beyond 3 mm, reaching approximately 2.8 eV at 4.5 mm. This indicates a maximum collision frequency region for a gas pressure of 100 Pa. A similar trend is observed at 150 ns; temperature increasing to 4 eV, exhibiting a peak around 1 mm. Moreover, similar temperatures beyond 2 mm suggest that the plasma is likely in a quasi-steady state because the plasma is surrounded by 100 Pa H_2 gas, although further analysis of atomic and molecular processes is required.

Prominent Sn I (452.47 nm) and Sn II (457.9 nm) emission lines observed between 400 and 600 nm were analyzed to investigate the plasma dynamics following laser irradiation. The spatiotemporal distributions of Sn I (452.4 nm) and Sn II (458 nm) emissions were analyzed by constructing contour maps (Fig. 5). In vacuum, Sn II emission extends up to approximately 16 mm and lasts for ~ 440 ns, whereas Sn I emission is confined to within ~ 7 mm and only the near-surface plasma persists longer than 250 ns. In a hydrogen atmosphere, the Sn I emission region expands considerably, almost covering the field of view (< 15 mm), whereas the Sn II emission area becomes markedly smaller. Multicharged ions undergo recombination and charge exchange reactions during laser plasma expansion, resulting in the creation of low-charge ions and neutral atoms. In addition, the electrons suffer from cooling owing to collisions with the H_2 ambient gas. As a result, the hot dense laser plasma approaches a nonequilibrium condition (low temperature and high density), where a three-body collisional recombination, such as $Sn^+ + e + e \rightarrow Sn^* + e$, becomes the dominant reaction. Sn* corresponds to the high Rydberg level. The electrons captured in these states undergo collisional decay to lower ones and subsequently undergo radiative decay, emitting intense radiation. These neutral Sn atoms may further react with hydrogen radicals to form SnH_4 [9].

In a hydrogen atmosphere, the plasma generated by the laser irradiation of the Sn target exhibits complex spatiotemporal dynamics. As shown in Fig. 6, the H_α line spectrum starts to emit during and immediately after laser irradiation. This suggests that diverse excitation mechanisms exist, i.e., photoexcitation owing to X-rays, EUV, and VUV, and electron impact excitation owing to energetic ones expanding from the laser plasma. However, after laser irradiation, the photoexcitation ceases and expanding thermal electrons have sufficient energy to dissociate and excite/ionize the hydrogen molecules

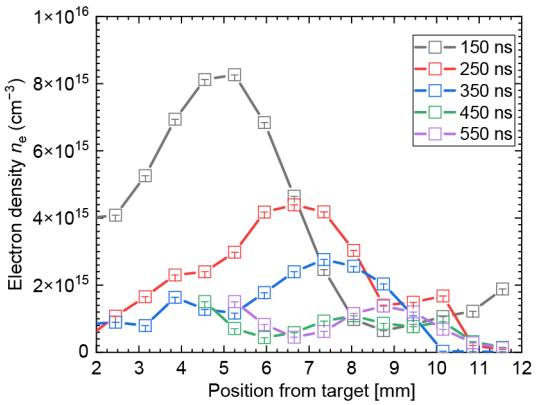

Fig. 7. Dependence of distance from the target on electron density at various time delays.

and atoms. In fact, the H_α emissions were observed far from the target surface.

Electron density was determined using the H_β Stark width. The FWHM of the Stark broadening spectrum, $\Delta\lambda_s$, is as follows [10]:

$$\Delta\lambda_s[\mathrm{nm}] = 4.8 \times \left(\frac{n_e[\mathrm{m}^{-3}]}{10^{23}[\mathrm{m}^{-3}]} \right)^{0.68}. \quad (1)$$

Figure 7 shows the dependence of electron density on the target position for various time delays. The electron density is as high as 1×10^{16} cm^{-3} at a 150-ns time delay and 5-mm distance from the target position. The electron density emission peaks shifted toward the right side with time. From the relation between the peak position and time delay, we can determine the electron expansion velocity, yielding ~ 1.5×10^4 m/s for the 150–250-ns time interval. On closer inspection, two peaks appear for each time delay. Although the reason for this is unclear, the first peak, which is closer to the target, is attributable to energetic electrons, while the second peak is attributable to thermal electrons.

4. Conclusion

Herein, the characteristics of laser-produced tin and hydrogen plasma were investigated in vacuum and a 100 Pa hydrogen atmosphere. By measuring the spatiotemporal visible emission, the dynamic behavior of atomic and ionic Sn and hydrogen species was examined.

The results revealed that hydrogen plasma was formed over a wide spatiotemporal range and the introduction of hydrogen gas considerably altered the emission behavior of Sn ions and atoms. Sn spectra revealed that plasma recombination is crucial for enhancing neutral emissions while reducing those from ions. Meanwhile, hydrogen atomic emission suggested that photoexcitation and electron impact excitation processes contributed to hydrogen dissociation and excitation. The photoexcitation could be driven by XUV or VUV radiation from the Sn plasma, typically occurring at 30–40 eV during or immediately after the picosecond laser pulse.

The Te of the generated Sn plasma was within the typical range of 2–5 eV, confirming the formation of a conventional laser-produced plasma. In a hydrogen atmosphere, the Te gradually decreased from approximately 4 eV, consistent with the spatiotemporal behavior of atomic hydrogen emission. Similarly, the electron density showed a typical value of approximately 10^{16} cm^{-3}, and a region with nearly constant density remained for approximately 150 ns after laser irradiation, matching the hydrogen emission region.

Future studies incorporating higher temporal-resolution spectroscopy and complementary ion detection methods will be necessary to determine plasma parameters at earlier times and establish a highly comprehensive understanding of the reaction mechanisms, including their role in SnH_4 formation.

[1] R. Garza *et al.*, J. Vac. Sci. Technol. A **41**, 063209 (2023).
[2] D. Qerimi *et al.*, J. Appl. Phys. **132**, 113302 (2023).
[3] J.P. Allain *et al.*, SPIE 6517, Emerging Lithographic Technologies XI, 65171V (2007).
[4] H. Komori, SPIE **5374**, 710 (2000).
[5] P. Mirkarimi, Appl. Opt. **39**, 1617 (2000).
[6] V. Bakshi, *EUV Sources for Lithography*, (SPIE Press, Bellingham, WA, 2006).
[7] S. Namba *et al.*, J. Appl. Phys. **104**, 013305 (2008).
[8] O.O. Versolato, Plasma Sources Sci. Technol. **28**, 083001 (2019).
[9] S. Namba *et al.*, J. Appl. Phys. **99**, 073302 (2006).
[10] M.A. Gigosos *et al.*, Spectrochim. Acta B **58**, 1489 (2003).